Inferring CO2 sources and sinks from satellite observations: Method and application to TOVS data

F. Chevallier, M. Fisher, Philippe Peylin, S. Serrar, Philippe Bousquet, Francois-Marie Breon, A. Chedin, Philippe Ciais

Inferring CO_2 sources and sinks from satellite observations: Method and application to TOVS data

F. Chevallier,[1] M. Fisher,[2] P. Peylin,[3] S. Serrar,[1,4] P. Bousquet,[1] F.-M. Bréon,[1] A. Chédin,[5] and P. Ciais[1]

Received 20 June 2005; revised 24 September 2005; accepted 27 October 2005; published 29 December 2005.

[1] Properly handling satellite data to constrain the inversion of CO_2 sources and sinks at the Earth surface is a challenge motivated by the limitations of the current surface observation network. In this paper we present a Bayesian inference scheme to tackle this issue. It is based on the same theoretical principles as most inversions of the flask network but uses a variational formulation rather than a pure matrix-based one in order to cope with the large amount of satellite data. The minimization algorithm iteratively computes the optimum solution to the inference problem as well as an estimation of its error characteristics and some quantitative measures of the observation information content. A global climate model, guided by analyzed winds, provides information about the atmospheric transport to the inversion scheme. A surface flux climatology regularizes the inference problem. This new system has been applied to 1 year's worth of retrievals of vertically integrated CO_2 concentrations from the Television Infrared Observation Satellite Operational Vertical Sounder (TOVS). Consistent with a recent study that identified regional biases in the TOVS retrievals, the inferred fluxes are not useful for biogeochemical analyses. In addition to the detrimental impact of these biases, we find a sensitivity of the results to the formulation of the prior uncertainty and to the accuracy of the transport model. Notwithstanding these difficulties, four-dimensional inversion schemes of the type presented here could form the basis of multisensor data assimilation systems for the estimation of the surface fluxes of key atmospheric compounds.

Citation: Chevallier, F., M. Fisher, P. Peylin, S. Serrar, P. Bousquet, F.-M. Bréon, A. Chédin, and P. Ciais (2005), Inferring CO_2 sources and sinks from satellite observations: Method and application to TOVS data, *J. Geophys. Res.*, *110*, D24309, doi:10.1029/2005JD006390.

1. Introduction

[2] The monitoring of carbon dioxide fluxes at the Earth's surface has become a major scientific challenge over the last few decades. It has progressed mainly through the exploitation of in situ measurements of CO_2 concentration at a network of ground stations. With the help of atmospheric transport information, inverse methods have been applied to deduce the patterns and amplitude of surface fluxes that generated the observed concentrations. However, with about 100 stations, the current network of surface stations provides scant information about the global-scale spatial and temporal variations of CO_2 fluxes, most particularly over land [e.g., *Gurney et al.*, 2002]. This situation is likely to improve: the surface observation network is being augmented, and efforts are being made to measure atmospheric CO_2 from space.

[3] The impact of CO_2 variations on some satellite records has been noticed for a long time [e.g., *Turner*, 1993, 1994], but CO_2 concentrations have been estimated from radiance measurements only recently. Retrieval methods were first applied to TOVS [*Chédin et al.*, 2003b] then to the Atmospheric Infrared Sounder (AIRS) [*Crévoisier et al.*, 2004; *Engelen et al.*, 2004]. Within the coming years, CO_2 retrievals are expected from the Infrared Atmospheric Sounding Interferometer (IASI) and the CO_2-dedicated Orbiting Carbon Observatory (OCO) and the Greenhouse Gases Observing Satellite (GOSAT).

[4] Such data contrast with the existing in situ measurements, and their nature will lead to a revolution in the methods of CO_2 flux estimation. First, they correspond to vertically integrated concentrations rather than point-wise observations. Second, the radiance information is ambiguous and the accuracy of instantaneous retrievals of column integrated CO_2 is not expected to be better than a couple of particles per million (ppm) [*Chédin et al.*, 2003c; *Dufour and Bréon*, 2003; *Engelen and Stephens*, 2004]. Third, the spatial density of the satellite data, which makes them attractive, increases the dimension of the observation vector

[1]Laboratoire des Sciences du Climat et de l'Environnement, Institut Pierre-Simon Laplace, Gif-sur-Yvette, France.
[2]European Centre for Medium-Range Weather Forecasts, Reading, UK.
[3]Laboratoire de Biogéochimie des Milieux Continentaux, Thivernal-Grignon, France.
[4]Also at Laboratoire de Météorologie Dynamique, Institut Pierre-Simon Laplace, Palaiseau, France.
[5]Laboratoire de Météorologie Dynamique, Institut Pierre-Simon Laplace, Palaiseau, France.

0148-0227/05/2005JD006390

by several orders of magnitude. Spatial and temporal averaging can reduce the dimension of the problem, but if one wants to use the information without degrading it, one faces new numerical problems.

[5] The goal of this paper is to define a methodology to estimate CO_2 surface fluxes using the combination of raw satellite retrievals and any prior information, like a flux climatology. This methodology follows the Bayesian framework, which has been widely used for the in situ network in a matrix form, but a variational formulation is chosen here, since it can cope with the dramatic increase of the number of data. The inference scheme is outlined in section 2. It is applied to the first CO_2 retrieval data set that has been compiled: the one from TOVS. Large regional biases have been identified in this product so that it barely agrees with forward model simulations using optimized surface fluxes (P. Peylin et al., manuscript in preparation, 2006). Therefore we focus here on the illustration of the method, in preparation for the analysis of forthcoming retrieval data, of potentially improved quality. The TOVS product and the prior information about the surface fluxes are described in section 3. Information about the atmospheric transport is provided by the global climate model of the Laboratoire de Météorologie Dynamique (LMD), which is called LMDZ (the last letter stands for "zoom capacity"). We nudge LMDZ toward the winds of the European Centre for Medium-Range Weather Forecasts (ECMWF), as discussed in section 4. Section 5 analyzes the behavior of the inference scheme in terms of (1) error reduction, (2) information content of the satellite data, (3) CO_2 flux and concentration increments, and (4) fit to ground measurements. Results are discussed in section 6 and conclusion follows in section 7.

2. Inference Scheme

2.1. Theoretical Framework

[6] In the following, the notations follow the convention defined by *Ide et al.* [1997]. Observation values are represented as a vector $\mathbf{y}$ and their error statistics are assumed to be unbiased and Gaussian with covariance matrix $\mathbf{R}$. Similarly, the prior information (or background) about the variables $\mathbf{x}$ to be optimized (here the CO_2 fluxes) is given by a vector $\mathbf{x}^b$ with unbiased Gaussian error statistics, described by the covariance matrix $\mathbf{B}$. A model H (here a transport model and a convolution operator) provides the equivalent of the observations $\mathbf{y}$ (here satellite CO_2 retrievals, but they could be in situ measurements as well) from the control variables $\mathbf{x}$. Errors of the forward model H can be taken into account in matrix $\mathbf{R}$.

[7] From the theory of Bayesian inference, it is well known that if H is a linear operator $\mathbf{H}$, the information about the variables $\mathbf{x}$, given the observations and the prior information, has Gaussian statistics as well, with mean $\mathbf{x}^a$ and covariance error matrix $\mathbf{A}$.

[8] The $\mathbf{x}^a$ and $\mathbf{A}$ can be computed in different ways [e.g., *Rodgers*, 2000]. One of them is as follows:

$$\mathbf{x}^a = \mathbf{x}^b - \mathbf{B}\mathbf{H}^T\left(\mathbf{H}\mathbf{B}\mathbf{H}^T + \mathbf{R}\right)^{-1}\left(\mathbf{H}\mathbf{x}^b - \mathbf{y}\right) \quad (1)$$

$$\mathbf{A} = \mathbf{B} - \mathbf{B}\mathbf{H}^T\left(\mathbf{H}\mathbf{B}\mathbf{H}^T + \mathbf{R}\right)^{-1}\mathbf{H}\mathbf{B}. \quad (2)$$

[9] After some algebra, equations (1) and (2) can be rewritten as follows, in order to change some of the dimensions of the matrices to invert:

$$\mathbf{x}^a = \mathbf{x}^b - \left(\mathbf{H}^T\mathbf{R}^{-1}\mathbf{H} + \mathbf{B}^{-1}\right)^{-1}\mathbf{H}^T\mathbf{R}^{-1}\left(\mathbf{H}\mathbf{x}^b - \mathbf{y}\right) \quad (3)$$

$$\mathbf{A} = \left(\mathbf{H}^T\mathbf{R}^{-1}\mathbf{H} + \mathbf{B}^{-1}\right)^{-1}. \quad (4)$$

[10] Alternatively, it can be shown that $\mathbf{x}^a$ is the minimum of the following quadratic cost function:

$$J(\mathbf{x}) = \frac{1}{2}\left(\mathbf{x} - \mathbf{x}^b\right)^T\mathbf{B}^{-1}\left(\mathbf{x} - \mathbf{x}^b\right) + \frac{1}{2}(\mathbf{H}\mathbf{x} - \mathbf{y})^T\mathbf{R}^{-1}(\mathbf{H}\mathbf{x} - \mathbf{y}). \quad (5)$$

[11] The minimum can be reached iteratively with a descent algorithm which requires several computations of the gradient of J with respect to the control variables $\mathbf{x}$:

$$\nabla J(\mathbf{x}) = \mathbf{B}^{-1}\left(\mathbf{x} - \mathbf{x}^b\right) + \mathbf{H}^T\mathbf{R}^{-1}(\mathbf{H}\mathbf{x} - \mathbf{y}). \quad (6)$$

[12] In this variational formulation of the inference problem, $\mathbf{A}$ is the inverse of the Hessian of J:

$$\mathbf{A} = \left(\nabla^2 J(\mathbf{x})\right)^{-1}. \quad (7)$$

[13] To summarize, the inference problem can be equivalently solved by matrix operations (equations (1)–(2) or (3)–(4)) or as the solution to a variational optimization problem (equations (5)–(7)).

2.2. Practical Implementation

[14] Practical considerations guide the choice between the matrix-based formulations and the variational approach. If the number of observations does not exceed a few thousands and if all elements of the matrix $\mathbf{H}$ are directly known, equations (1) and (2) provide the most straightforward solution. Conversely, equations (3) and (4) are more convenient to use when the number of control variables is small and $\mathbf{R}$ is easy to invert (e.g., $\mathbf{R}$ is diagonal). For large problems in both the observation space and the control variable space, the inversion of $(\mathbf{H}\mathbf{B}\mathbf{H}^T + \mathbf{R})$ or of $(\mathbf{H}^T\,\mathbf{R}^{-1}\,\mathbf{H} + \mathbf{B}^{-1})$ may be prohibitive. The variational framework still implies the inversion of $\mathbf{B}$ and $\mathbf{R}$, but in many applications these matrices are sparse, if not diagonal. More generally, it is simpler to make convenient assumptions about $\mathbf{B}$ and $\mathbf{R}$ to make them easy to invert than it is for $(\mathbf{H}\,\mathbf{B}\mathbf{H}^T + \mathbf{R})$ and $(\mathbf{H}^T\,\mathbf{R}^{-1}\mathbf{H} + \mathbf{B}^{-1})$. Still, the implementation of the variational approach for large problems would stumble on the multiplication of $\mathbf{H}^T$ by $\mathbf{R}^{-1}(\mathbf{H}\mathbf{x} - \mathbf{y})$ in the expression of ∇J (equation (6)) without the adjoint technique [e.g., *Errico*, 1997]. This approach avoids the explicit calculation of all the elements of $\mathbf{H}$ by decomposing $\mathbf{H}^T$ into a product of elementary operations $\mathbf{H}^T = \prod_{i=n}^{1}\mathbf{H}_i$, with $\mathbf{H}_i$ being the Jacobian matrix of the ith line among n of the computer code of H. A single pass of the adjoint model computes $\mathbf{H}^T\,\mathbf{R}^{-1}(\mathbf{H}\mathbf{x} - \mathbf{y})$, which is added to $\mathbf{B}^{-1}(\mathbf{x} - \mathbf{x}^b)$ to give ∇J (equation (6)).

[15] Up to now the estimation of CO_2 surface fluxes at the global scale has relied on the matrix formulation [e.g., *Bousquet et al.*, 2000; *Gurney et al.*, 2002; *Rödenbeck et al.*, 2003]. This paper reports on the implementation of the

variational approach in order to deal with large numbers of observations and control vector dimensions of several hundred thousands. The minimization strategy follows the one chosen for the ECMWF four-dimensional variational analysis system (4D-Var). The ECMWF 4D-Var minimization algorithm is based on the Lanczos version of the conjugate gradient algorithm [*Lanczos*, 1950] that advantageously provides the leading eigenvectors of the Hessian $\nabla^2 J(\mathbf{x})$ as a byproduct of the minimization [*Fisher and Courtier*, 1995]. For efficiency, the minimization is preconditioned by defining the variable to optimize as

$$\chi = \mathbf{B}^{-1/2}\mathbf{x}. \quad (8)$$

[16] The reader is referred to *Trémolet* [2004] and references therein for a description of other features of the ECMWF 4D-Var. The ECMWF minimization algorithm has also been implemented for data assimilation in an ocean model [*Weaver et al.*, 2003].

2.3. Inferred Variables

[17] In this study, the control vector $\mathbf{x}$ contains the CO_2 surface fluxes to be inferred. Most inversions performed in the past have used monthly or even annual fluxes. Very few attempts have been made towards subdiurnal fluxes so far [*Law et al.*, 2004]. In the method described here, most of the computational burden (CPU and memory) is caused by the transport model, the performance of which is not affected by a change of the time discretization. However, the choice of the time resolution may affect the number of iterations of the minimization. It also bears consequences on the definition of the prior errors because these are likely to be temporally correlated if the resolution is high. In the results presented here, fluxes are arbitrarily inverted as monthly averages, but a major submonthly variation is accounted for by defining daytime (i.e., from local sunset to sundown) and nighttime monthly fluxes separately. This allows a simple optimization of the biosphere diurnal cycle amplitude, some features of which are noticeable in the TOVS observations [*Chédin et al.*, 2005]. Note that it partly addresses the issue raised by *Rayner et al.* [2002] of biases caused by a poor sampling of the diurnal cycle by measurements.

[18] Conversely, the spatial resolution of the fluxes in the control vector is a compromise. It seems important to give some freedom to the inference system to adjust small-scale patterns, by specifying fluxes at the highest possible horizontal resolution (i.e., that of the transport model) [e.g., *Kaminski et al.*, 2001]. On the other hand, prior flux errors are more likely to be correlated from one cell to another at high horizontal resolution than at low. In the past, fluxes have been inferred over large regions, mainly for computational reasons that are not relevant here. Therefore fluxes are defined in this study on the horizontal grid of the transport model, which is regular with 96 points in longitude and 72 in latitude (i.e., a $3.75^\circ \times 2.5^\circ$ longitude-latitude grid).

[19] It is also important to give some freedom to the analysis system to adjust the CO_2 concentration field at the initial time step of the assimilation window in order not to alias its errors into flux errors. To do so, the three-dimensional (3-D) concentration field of CO_2 concentrations at the initial time step could be included in the control vector $\mathbf{x}$. Since we do not focus here on the analysis of this field, and in order not to unnecessarily increase the array dimension, only the initial total CO_2 atmospheric columns at each grid point of the $3.75^\circ \times 2.5^\circ$ grid are introduced in the control vector.

[20] The dimension of the control vector for an assimilation window covering a whole year is about 200,000 (i.e., two times the number of grid points for the day and night fluxes, times the number of months, plus the number of grid points for the concentration field at initial time).

3. Observations and Prior Information

3.1. TOVS CO_2 Retrievals

[21] TOVS instruments have been operating since 1979 on board the polar-orbiting satellites of the National Oceanic and Atmospheric Administration (NOAA). Some of its channels at infrared wavelengths are noticeably impacted by CO_2 variations, in particular in the upper troposphere. Upper tropospheric CO_2 retrievals from the NOAA-10 spacecraft have recently been produced for the tropical region (25°S–25°N). Farther away from the equator, the lower position of the tropopause, its warmer temperature and the larger variability of the temperature profile in the vertical prevent the extraction of the CO_2 signals. Clouds impede the inversion and the method is restricted to clear-sky spots. Even so, more than 100,000 retrievals at spatial resolution of about 100×100 km^2 are gathered per month of NOAA-10 observation. NOAA-10 is a Sun-synchronous polar satellite. Its archive covers the period between November 1986 and September 1991, but only year 1990 is processed here. During that year NOAA-10 orbits crossed the equator at about 0740 and 1940 local solar time, which allows two samples of the diurnal cycle.

[22] The column-CO_2 inversion algorithm is an artificial neural network of the type defined by *Rumelhart et al.* [1986]. This nonlinear regression has been trained from the Thermodynamical Initial Guess Retrieval (TIGR) [*Chédin et al.*, 1985; *Chevallier et al.*, 1998] climatological data set, previously extended to include variable atmospheric CO_2 concentrations. The regression estimates a weighted mean CO_2 concentration between the tropopause and about 400 hPa, with a maximum weight at about 200 hPa (Figure 1). Individual retrievals are used here, in contrast to *Chédin et al.* [2003b], who averaged the retrievals in both time and space to study them.

3.2. Previous Validations

[23] The LMD TOVS retrievals [*Chédin et al.*, 2003b] have been the first attempt to describe the CO_2 concentrations in the upper troposphere and in the tropical band directly from the observations. This pioneering effort has been followed by the evaluation of the product, based on comparisons with the few aircraft campaigns available, with models, and on sensitivity studies. The conclusions of this evaluation can be summarized as follows: (1) the retrievals adequately identify CO_2 variations (the growth rate interannual variations, for example) only when averaged over at least a month and over very large regions [*Chédin et al.*, 2003b]; (2) the limited information contained in the TOVS radiances does not allow the separation between CO_2 variations and those of other atmospheric signals, like ozone variations, over smaller spatial and temporal scales; (3) such regional biases, however, have less of an impact on the

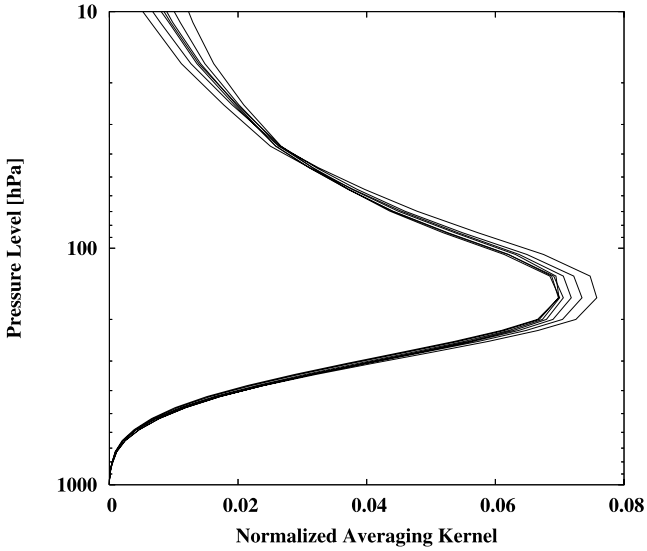

Figure 1. Normalized averaging kernel of the TOVS CO_2 retrieval for seven different viewing angles of the TOVS instrument. The averaging kernel is defined here as $\partial\tilde{c}/\partial c(P)$, where $\tilde{c}$ is the retrieval, $c(P)$ is the CO_2 atmospheric concentration at pressure level P. $\tilde{c}$ and $c(P)$ are expressed in ppm Pa^{-1}. The averaging kernel has been estimated by finite differences based on model simulations.

12-hour difference between daytime and nighttime retrievals and a consistent link between this difference and biomass burning emissions at regional scale has been established [*Chédin et al.*, 2005].

[24] From these previous studies, one can foresee that surface fluxes inferred from TOVS would be affected by some regional biases induced by those of the retrievals. The TOVS data are used here as a testbed for a methodology that will be applied to the forthcoming retrievals, from AIRS and OCO, for instance.

3.3. Observation Error Covariance Matrix

[25] The observation error covariance matrix **R** is a key component of the retrieval system (equations (5)–(6)) and a proper assessment of its elements, i.e., variances and correlations, is needed. As mentioned above in section 2.1, **R** takes the errors of H into account in addition to the measurement errors. Local time and space variations of LMDZ CO_2 concentrations are used here as a surrogate for representativeness errors, following the approach described by *Rödenbeck et al.* [2003]. Practically, for each model grid point and for each model time step, a standard deviation is computed for 16 values of the LMDZ simulation that uses the prior fluxes. The 16 values correspond to the eight latitude/longitude grid points surrounding the observation at the start of the time step and to the eight ones at the end. Representativeness error is defined as the monthly average of these standard deviations and the corresponding variances (typically a few tenths of ppm for upper-tropospheric observations) are added to the ones of the retrieval error. Correlations of the representativeness error are neglected.

[26] Previous studies of the TOVS retrievals have focussed on monthly means at a horizontal resolution of $15° \times 15°$ and the corresponding estimations of the product errors [e.g., *Chédin et al.*, 2003b] are not relevant for the present one that uses individual retrievals. Accurate independent observations of CO_2 concentrations in the upper troposphere would be useful to build global statistics. For instance, an estimate of the error variance may be based on aircraft measurements, but these are too sparse for an estimation of the error correlations. To circumvent this problem, model simulations are used here. Atmospheric profiles (temperature, humidity, and ozone) and surface characteristics (temperature) have been extracted from the ECMWF archive. The fields correspond to the operational analyses valid at 1200 UTC every 5 days for 365 days starting on 1 November 2003. The profiles are described on 60 vertical levels. Only grid points whose latitude lies within 25° from the equator and with upper tropospheric relative humidity below 70% (i.e., about cloud-free at these altitudes) are kept. Together with a constant atmospheric CO_2 concentration of 370 ppm, those fields are used as input to two radiation models, depending on the wavelength of the TOVS channels. The first one is the narrow-band model Synsatrad [*Tjemkes and Schmetz*, 1997] that simulates here the TOVS infrared channels. The 3R-N model [*Chédin et al.*, 2003a] is another radiation model, applied here to the TOVS microwave channels. Synsatrad and 3R-N produce a set of simulated radiances, to which an estimate of the TOVS instrument noise is added (in the form of a Gaussian random perturbation). CO_2 concentrations are then retrieved from those pseudodata by the same artificial neural network that processed the TOVS archive. Finally, the retrievals are compared to the initial "true" CO_2 value (370 ppm). The differences are interpreted as retrieval errors. Note that the artificial neural network training made use of only the 3R-N model for both infrared and microwave channels [*Chédin et al.*, 2003b]. The introduction of an independent model, i.e., Synsatrad, for the present study can be seen as a surrogate for infrared spectroscopic errors.

[27] The standard deviation of differences between the input to the radiation models and the output of the neural network reach 5.7 ppm for individual data. By consequence, variances of the TOVS retrieval errors are set to 36 ppm^2 here. Note that this is error corresponds to individual retrievals, in contrast to the previous studies [e.g., *Rayner and O'Brien*, 2001] that used observations temporally averaged.

[28] Figure 2 displays the correlations of the differences as a function of the ground distance between two retrievals.

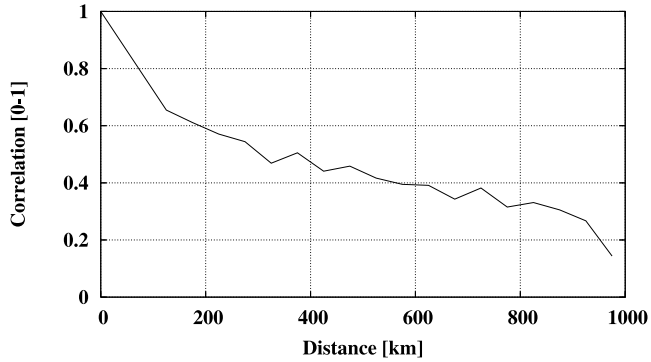

Figure 2. Correlation of the TOVS retrieval errors as a function of the ground distance.

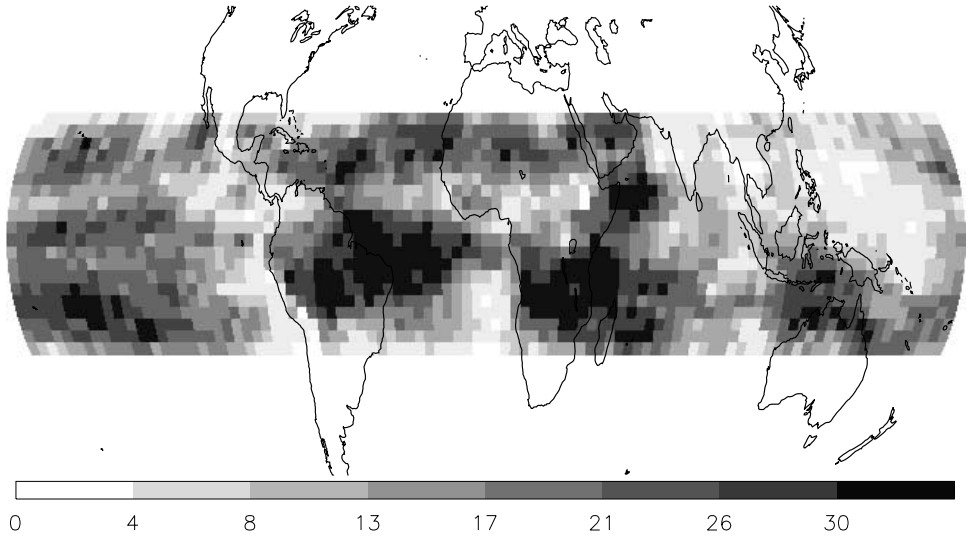

Figure 3. Number of TOVS observations in each grid box of the LMDZ transport model after spatial filtering for August 1990.

By comparison, the transport resolution in this study is about 400 km along a parallel and 280 km along a meridian in the tropical belt. One may note that the error correlations are attenuated by as much as a twofold factor within about 500 km, i.e., from one grid point to about the next. Consequently, the following methodology is defined in the present study. TOVS data are subsampled so that each model grid point contains no more than one TOVS observation per grid point within any 6-hour time window and correlations between the selected observations are neglected. This approximation makes the covariance matrix **R** diagonal which simplifies the inference scheme.

[29] To limit the impact of ozone-related regional biases (see section 3.2), a quality control has been introduced that aims at removing the data in the presence of ozone extrema. Large ozone values in the upper troposphere are usually associated with stratospheric intrusion and are flagged here by a threshold on the absolute value of the potential vorticity on the 350 K isentropic surface. This threshold is 1 PVU = 10^{-6} m^2 s^{-1} K kg^{-1}. Ozone-poor air is more difficult to diagnose indirectly. The lowest quarter of the retrieved CO_2 values (i.e., less than 351 ppm for year 1990) were simply rejected since they may correspond to an ozone minimum aliased into a CO_2 minimum.

[30] The number of TOVS retrievals that passed both the spatial screening and the quality control is illustrated in Figure 3 for August 1990. Lower densities are observed in the cloud regions: mainly the intertropical convergence zone (ITCZ) and the stratocumulus areas off the West coast of the continents. In total 347,400 TOVS retrievals are used in the results presented here.

3.4. Background Flux Information

[31] For background information, we use direct estimates of the surface carbon fluxes, including anthropogenic and natural components. Fossil fuel CO_2 emissions are from the EDGAR-3.0 emission database [*Olivier et al.*, 1996]. The data set is based on a combination of statistics on energy consumption, emission factors, and population density maps, and the total emission was rescaled to 6.1 Gt C per year for the year 1990. Air-sea CO_2 exchange is prescribed from the study by *Takahashi et al.* [2002], where a climatological extrapolated distribution of sea-air pCO_2 differences and a wind-dependent gas exchange coefficient [*Wanninkhof*, 1992] have been combined to produce monthly air-sea fluxes. The biosphere-atmosphere exchange of CO_2 is estimated by the Terrestrial Uptake and Release of Carbon (TURC) model [*Lafont et al.*, 2002]. TURC is a simple model of the biosphere driven by radiation, temperature, and humidity fields from ECMWF and by the Fraction of Absorbed Photosyntetically Active Radiation (FAPAR) from the SPOT4-VEGETATION sensor. SPOT4-VEGETATION data for the period between March 1998 and March 1999 are used here. The calculated daily fluxes have been redistributed throughout the day to account for the diurnal cycle of the fluxes. We used a simple scaling scheme where Gross Primary Production follows the incoming shortwave radiation and local air temperature. Finally, the TURC model is forced to be carbon neutral on a yearly basis.

[32] Current flux measurements do not allow us to estimate the errors of these prior fluxes. The inference of CO_2 fluxes usually relies on ad hoc **B** matrices. Correlations are either neglected or specified per geotype as a function of the distance. Variances are either isotropic or specified from some biogeochemical considerations [e.g., *Bousquet et al.*, 2000; *Rödenbeck et al.*, 2003; *Houweling et al.*, 2004]. For instance they may be defined over land from a pattern of net primary productivity. The correlation lengths impose a smoothness constraint on the flux increments generated by the inversion system and the variance pattern favors some of the regions (i.e., the ones with the highest variance) for the increments to occur.

[33] We tested two background error matrices. First results have been obtained with a simple background matrix, where error correlations are set to zero. When using the error statistics of all pixels, corresponding specified standard deviations of the flux errors globally sum up to 1.2 Gt C per year only. They are spread in time and space proportionally to grid size. Error standard deviations equal

1%, for the total columns at initial time in each grid box. An alternate inversion has been based on a matrix more consistent with what we guess from the carbon cycle [e.g., *Rödenbeck et al.*, 2003]. In this configuration of the **B** matrix, correlation lengths are set to 1000 and 500 km over ocean and land, respectively, for both fluxes and total columns. Correlations in time for fluxes are set to zero. Corresponding specified standard deviations of the flux errors globally sum up to 2 and 5 Gt C per year for ocean and land, respectively, and are spread in time and space proportionally to grid size over ocean and to the heterotrophic respiration flux modeled by TURC over land. Standard deviations of CO_2 total columns errors are set to 1% in each grid box, as above.

[34] It turns out that the large misfit between the prior information and the TOVS data favors the simple **B** matrix, as will be described in the following. Therefore the presentation of the results will focus on this configuration. The tests with the matrix based on biogeochemical considerations are reported in section 5.4.

3.5. Global Concentration Offset

[35] Equations (1)–(7) implement the Bayes' theorem for the particular case of unbiased Gaussian statistics. The analysis is only supposed to account for random errors of the background and of the observations, as specified by the covariance matrices **B** and **R**. Biases therefore need to be removed from the inference system. Consistent with previous inversions, we calculate an offset of the atmospheric CO_2 by subtracting the mean of the departure statistics $\mathbf{Hx}_b - \mathbf{y}$ from the prior concentrations at the initial time step of the assimilation window.

4. Transport Model

[36] Atmospheric inversion studies usually consider CO_2 as a passive tracer. Indeed, CO_2 is a rather stable gas in the troposphere and its chemical production from reduced carbon compounds may reasonably be neglected. Further, basic CO_2 climatologies are sufficient to properly account for the impact of CO_2 variations on meteorology via radiation. Consequently, the observation operator **H** in equations (1)–(4) can be reduced to transport (large-scale and subgrid) processes and to a convolution operator.

[37] The present inference scheme relies on the off-line version of the LMDZ general circulation model [*Sadourny and Laval*, 1984; *Hourdin and Armengaud*, 1999]. This version computes the evolution of atmospheric compounds based on an archive of transport fields: winds, convection mass fluxes, and planetary boundary layer exchange coefficients. The archive is built from a prior integration of the complete general circulation model. In this study as in the one by *Hourdin and Issartel* [2000], the horizontal winds have been nudged toward ECMWF meteorological analyses during the preliminary simulation in order to realistically reproduce the actual meteorology.

[38] The complete LMDZ model solves the primitive equations on a 3-D eulerian grid. Nineteen sigma-pressure layers are used here to discretize the vertical axis. They correspond to a resolution of about 300–500 m in the planetary boundary layer (first level at 70 m height) and to a resolution of about 2 km at the tropopause. Large-scale advection of trace species follows the Eulerian framework described by *Hourdin and Armengaud* [1999]. Deep convection is parameterized according to *Tiedtke* [1989] and the turbulent mixing in the boundary layer is based on *Laval et al.* [1981].

[39] For comparison with the TOVS observations, the concentrations computed at their location are convolved with the function displayed in Figure 1.

[40] We investigated the retro-transport approach of *Hourdin et al.* [2005] to perform the adjoint operations in the inversion scheme (equation (6)). This approach exploits the time symmetry of Eulerian transport to minimize the development of the adjoint code. Unfortunately, the symmetry property does not strictly hold when space is discretized, as already discussed by *Hourdin et al.* [2005]. We found that the accuracy of such retro-transport computations is not high enough for minimization algorithms like the conjugate gradient, that strictly require the quadraticity of the function to optimize. The retro-transport may be suitable for more flexible minimization algorithms, but they are likely to need more iterations to converge.

[41] As a consequence, we manually coded the tangent-linear (**H**) and the adjoint ($\mathbf{H}^T$) operators that correspond to the off-line version of LMDZ, line by line in order to reach the accuracy of the computer. Correctness of those models has been checked with the Taylor formula and by the identity between inner products that mathematically defines an adjoint.

5. Results

[42] The inference scheme was run for the entire year 1990 at once. Thirty iterations were used, which reduced the norm of the gradient by 10,000 times. The 30-iteration minimization required about 15 CPU days on an Intel P4 3 GHz processor. Note that the 10,000-fold reduction is theoretical because the minimization uses the tangent-linear of the nonlinear transport model. The actual reduction of the norm is a factor 42 only. It is possible to iterate on the linearization point as is done in the "outer loop" of the ECMWF 4D-Var [e.g., *Trémolet*, 2004] in order to come closer from the global minimum of the cost function. Tests of such an approach with the TOVS data did not significantly affect the results from the first minimization and are not reported in the following.

5.1. Estimation of the Error Reduction on the Surface Fluxes

[43] As mentioned in section 2.2, the Lanczos minimization scheme provides the leading eigenvectors of the second derivative of the cost function. The number of estimated eigenvectors is less than the number of iterations performed. From equation (7), the error reduction from the background to the analysis can then be estimated as a truncated eigenvector expansion [*Fisher and Courtier*, 1995]. This property is exploited in the ECMWF analysis system to precondition the minimization and to estimate analysis error variance [*Fisher and Andersson*, 2001]. The accuracy of the error estimate increases with the number of eigenvectors used, but this must be offset against the computational cost of increasing the number of minimization iterations. Using more eigenvectors decreases the analysis error estimate so

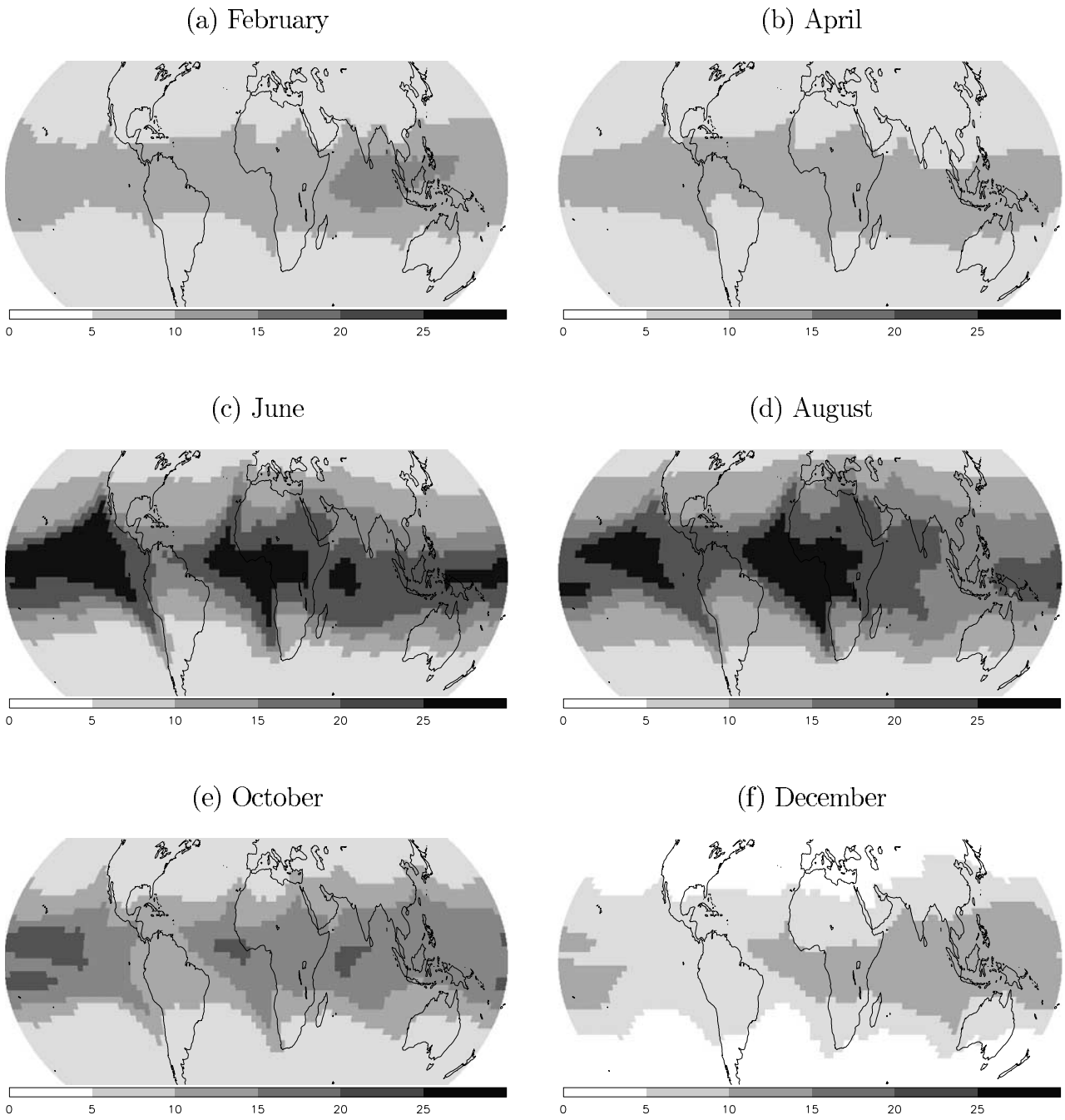

Figure 4. Truncated estimate of the reduction of CO_2 daytime flux errors (in g C per m^2 per year) for 6 months of year 1990, as delivered by TOVS CO_2 retrievals. The error reduction is defined as the square root of the difference between the background error variances and the analysis error variances. As explained in the text, only the patterns are relevant; values are underestimated further to the truncation (10 eigenvectors are used out of about 200,000).

that a truncated approximation is an overestimate of the analysis error variance implied by the assumed statistics of observation and background errors.

[44] Figure 4 displays such an estimate of the analysis error reduction for the daytime surface fluxes and for 6 months. The leading eigenvalue of the Hessian $\nabla^2 J(\chi)$ equals 1342 and the smallest eigenvalue retrieved is 30, knowing that by definition of χ (equation (8)) the eigenvalue spectrum further converges down to unity. The truncated eigenvector expansion provides those features of the error variance that have the largest spatial and temporal scales. Note that the error reduction is not related much to the observation location (Figure 3) and even expands in the midlatitudes. The error reduction is tightly linked with the main patterns of the general circulation in the tropics. The truncated error reduction is the largest in the ITCZ and in the trade wind regions that converge to this zone. The ascending branch of the Hadley circulation, which rapidly lifts air parcels from the

boundary layer to the upper troposphere, obviously drives the analysis. Note that observations are restricted to clear sky here and sample the air outflowed from the tropical convection rather than the air in the convective towers themselves. The transport between other source regions, such as the subtropical high-pressure systems, and the upper troposphere is much slower and the flux analysis is consequently weakly constrained there. Comparing the error reduction for each month of the year, one can see a seasonal variation, with the largest signal in boreal summer, and the weakest in boreal winter, which follows the variations of the ITCZ intensity. Similarly, the fluxes are characterized by a smaller error reduction during the night (when convection is the weakest) than during the day (not shown) even though the number of daytime TOVS observations is about the same as the number of nighttime ones.

[45] Additional iterations would increase the estimated error reduction and introduce smaller-scale patterns, but, by construction, they would not change the large-scale ones shown here. The Lanczos minimization scheme therefore gives an interesting, though incomplete, indicator of the theoretical error reduction.

5.2. Estimation of the Satellite Information Content

[46] As described by *Fisher* [2003], the Lanczos minimization algorithm also allows accurate estimation of two important measures of the observation information content. The first one is the degree of freedom for signal, expressed as [e.g., *Rodgers*, 2000]:

$$d = trace\left(\mathbf{I} - \mathbf{A}\mathbf{B}^{-1}\right) \tag{9}$$

$$= N - \sum_i \lambda_i, \tag{10}$$

where $\mathbf{I}$ is the identity matrix, N is the dimension of the control vector $\mathbf{x}$, and λ_i are the eigenvalues of $\mathbf{A}\mathbf{B}^{-1}$. The degree of freedom for signal describes the number of independent pieces of information that the observations provide, given the prior information.

[47] The second measure of the observation information content is given by the entropy reduction [e.g., *Rodgers*, 2000]:

$$S = -\frac{1}{2}\log_2\left|\mathbf{A}\mathbf{B}^{-1}\right| \tag{11}$$

$$= N - \sum_i \log_2(\lambda_i), \tag{12}$$

where S is the number of states, in bits, that can be distinguished using the observations in the space defined by the uncertainty of the prior information (whose metric is given by $\mathbf{B}$).

[48] Note that Bayesian estimation shows how observations improve the knowledge about chosen variables: it is relative to some prior information. Consistently, d and S depend on the errors of the prior.

[49] *Engelen and Stephens* [2004] studied the information content of the TOVS and AIRS radiance observations to infer CO_2 concentrations, based on those two quantities. The present study considers the step beyond, where surface fluxes are inferred. The dimension of this problem makes the estimation of $\sum_i \lambda_i$ and $\sum_{ii} \log_2(\lambda_i)$ difficult. However, the change of variables defined by equation (8) implies that the λ_is are the eigenvalues of $\nabla^2_\chi J(\mathbf{x})$, the leading ones being provided by the minimization algorithm. Moreover, the approach of *Bai et al.* [1996] allows to circumvent the unavailability of the trailing ones [*Fisher*, 2003].

[50] This approach has been applied to the 1990 TOVS data. Within 15 iterations, the entropy reduction converged to 341 and the degree of freedom for signal to 339. The former figure indicates that about 2^{341} states of the control vector (that can take an infinite number of values for each one of its 200,000 components) can be distinguished from a year's worth of TOVS data, given the specified prior information. The degree of freedom for signal allows the examination of the information content in the space of the observations. It shows that about 339 independent quantities can be measured from that year of TOVS data, given the specified prior information. One may compare the 339 independent quantities to the total number of observations available: 347,400. If these 339 information pieces were regularly spread between 20°S and 20°N and throughout the year (which is a rough approximation, as can be seen in Figure 4), each one of them would cover a 22.5° × 22.5° latitude-longitude surface. This simple calculation highlights the rather low resolution of the information about the CO_2 surface fluxes that can be extracted from upper tropospheric measurements. This rather low resolution stems from the highly diffusive nature of the atmosphere dynamics. Note that *Chédin et al.* [2003b, 2005] independently used the TOVS retrievals at resolution 15° × 15°, which is rather comparable to the present rough estimation. To summarize, given the specified errors of the observations and of the prior, the 347,400 CO_2 retrievals for year 1990 actually consist of 339 independent observations that allow to distinguish between 2^{341} states of the flux vector.

5.3. Optimized Concentrations and Fluxes

[51] The daytime flux increments for the 1990 analysis described above are illustrated in Figures 5 and 6: April and August values are presented. In the same figures, the background fluxes, the mean CO_2 fields in the background, the analysis and the observations are displayed as well. As expected (section 3.2), large differences can be seen between the background and the observation. The range for TOVS is about 7–9 ppm, with pronounced minima over the equatorial Pacific and in the subtropics in August. In contrast, the background mainly varies as a function of latitude within 4 ppm in April and 2 ppm in August. For each month shown, the analysis is a trade-off between the prior field and the observations, the weight of each being determined by the corresponding error covariance matrices and by the Jacobian of the transport model. The inference scheme adjusts the large-scale CO_2 patterns to fit the observations better for August than for April, consistent with the theoretical error reduction discussed in the previous section.

[52] The corrections to the surface fluxes occur throughout the tropics (Figures 5e and 6e), spreading beyond the areas where the error diminishes the most as estimated in

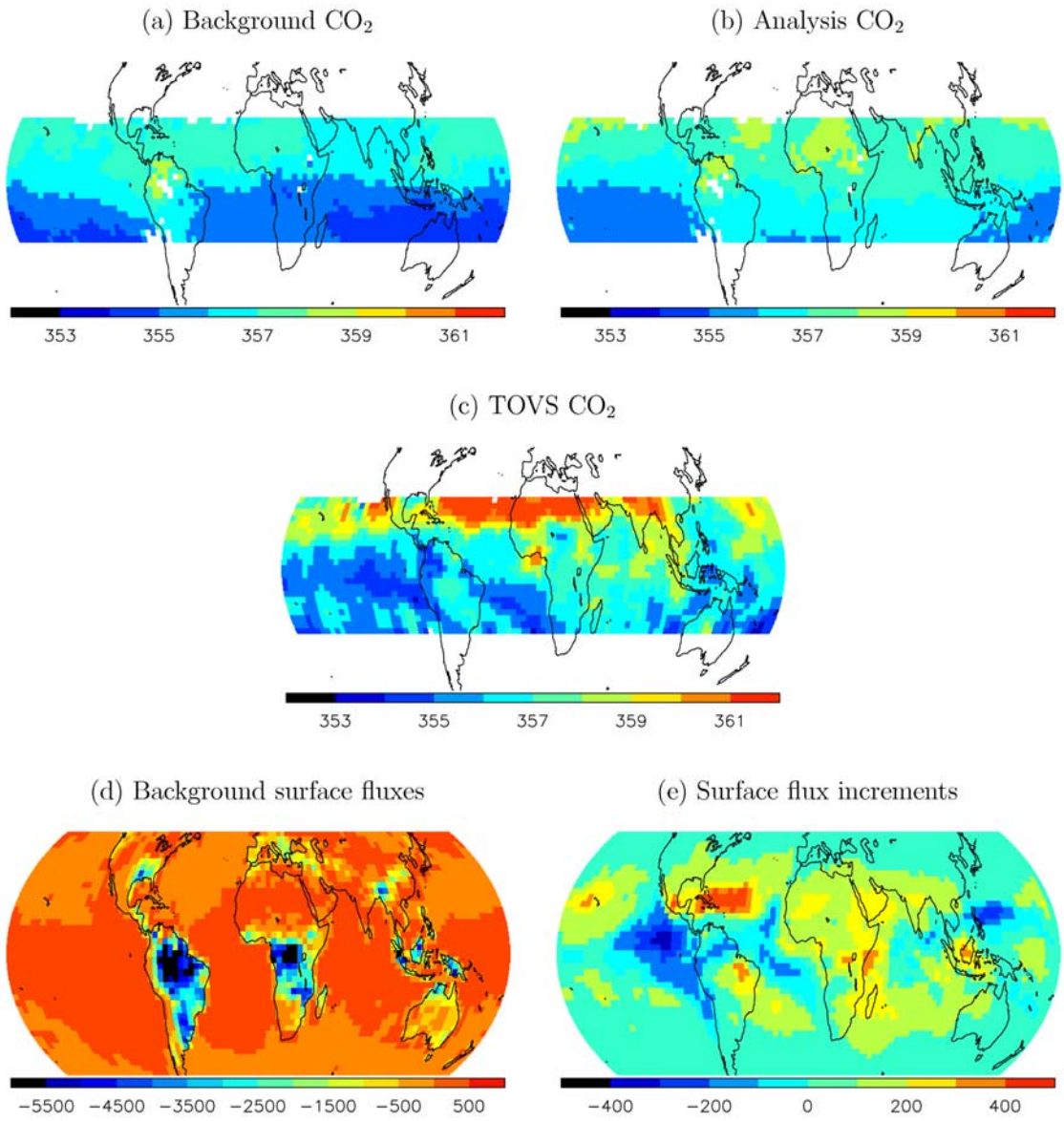

Figure 5. (a) Mean background, (b) analysis, and (c) TOVS CO_2 concentrations, in ppm, for April 1990 (d) and daytime flux background values and (e) increments (analysis minus background), in g C per m^2 per year, for 1 April 1990.

Figure 4. The offset correction on the concentrations mentioned in section 3.5 makes the annual global averages of the flux increments close to zero, but locally the annual mean reaches several hundreds g C per m^2 per year, which is one order of magnitude larger than the increments obtained from the analysis of surface in situ measurements [e.g., see *Rödenbeck et al.*, 2003, Figure 8d]. The mismatch of about 4 ppm in the upper troposphere above the central Pacific implies an increment of the order of 3 GTC yr^{-1} over the eastern equatorial Pacific with LMDZ. Some of the increment patterns are clearly not realistic, since carbon uptake is inferred from the TOVS analysis in some of the tropical oceans, in contradiction with the ocean pCO_2 observations in these relatively well-observed basins [*Takahashi et al.*, 2002].

[53] The flux increments are further evaluated against surface observations that are independent from the analysis (i.e., only the TOVS data are assimilated). To do so, we successively prescribed the prior and the analyzed fluxes as the boundary condition for the LMDZ transport model. The resulting monthly means of simulated CO_2 concentrations are compared to the values reported in the Globalview data set for a series of ground stations [*Globalview-CO_2*, 2004]. The Globalview monthly means are averages of smoothed measurements made at these observatories. The 1990 time series at three stations are shown in Figure 7 as an illustration. Table 1 summarizes the results by presenting the RMS statistics of the fit of the background and of the analysis to the Globalview monthly means for 1990 and 2003. The mean offset averaged over all the stations has been removed before the RMS computation. The prior RMS differences are usually about a couple of ppm. The analysis usually degrades them by a few tenth of ppm, except in the southern hemisphere, where the seasonal cycle is very small

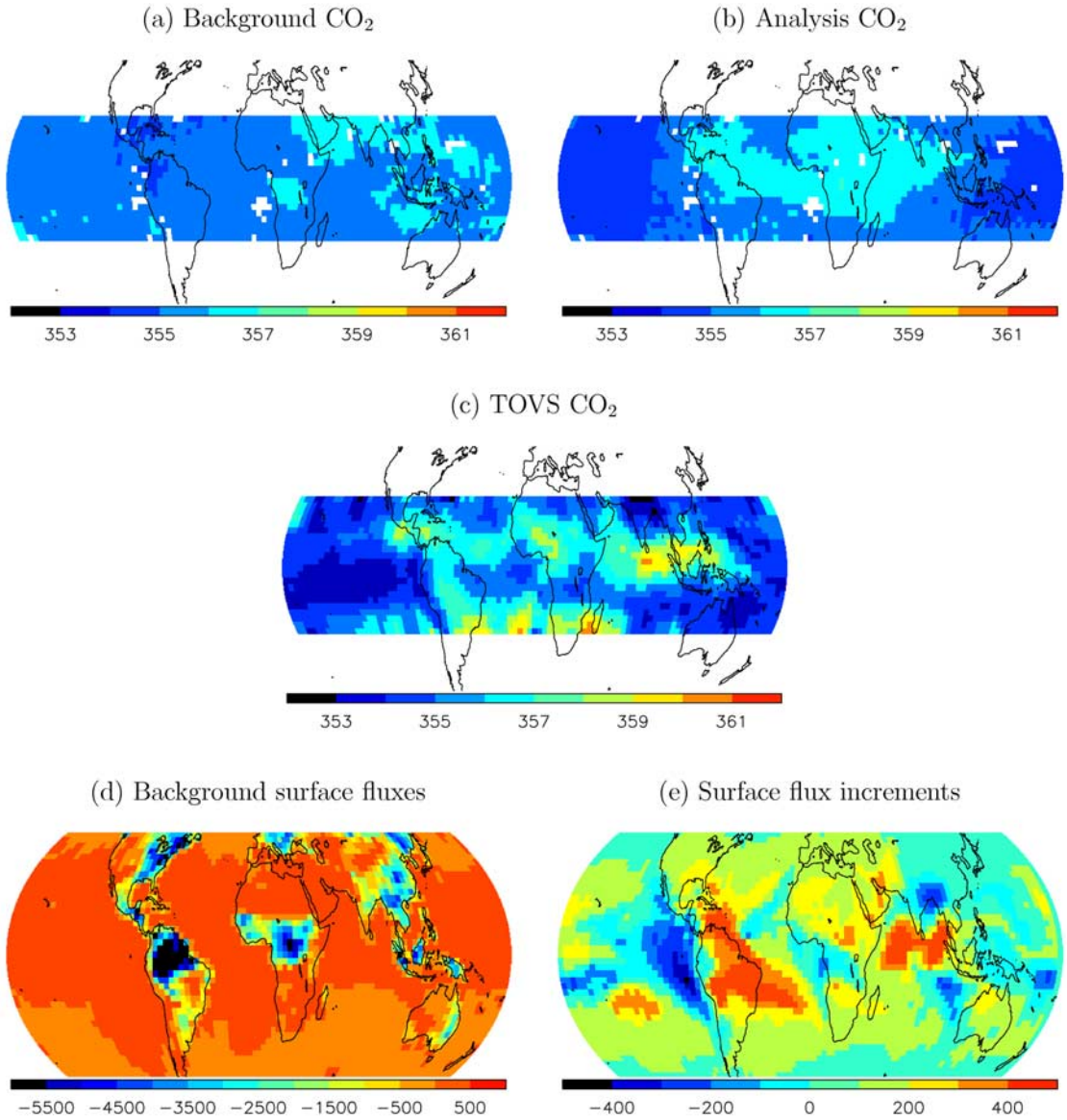

Figure 6. Same as Figure 5 for August 1990.

(so that the RMS difference is driven by its bias component). The conclusion of this evaluation is that, as expected (see section 3.2), the flux patterns inferred from the TOVS satellite observations using the LMDZ model are less accurate than the prior fluxes.

5.4. Alternate Specification of the Background Errors

[54] Results presented so far have relied on a crude specification of background flux errors, where correlations are neglected and where the same error (10^{-4} kg C per m^2 per hour) is attributed to each grid point flux. Complementary inversions have been performed with background errors from biogeochemical considerations, as described in section 3.4.

[55] The main features of this alternate inversion with respect to the results presented can be summarized as follows. First, the analysis fit to the CO_2 observations is about the same (2.7 ppm RMS difference in both cases). Second, the maps of theoretical error reduction reproduce the prescribed patterns of the prior error variance (here the heterotrophic respiration fluxes) in the tropics as at midlatitudes (Figure 8). Third, large flux increments occur at most latitudes with significant regional positive-negative dipoles (not shown). Fourth, the fit to the Globalview data set is further degraded.

[56] The realism of the analyzed fluxes appears to be less than with the diagonal background error matrix. This can be explained by the strong dipole increments needed to fit the biased TOVS data, while a distinction is made now between areas of high prior errors and areas of low ones.

[57] Note that *Houweling et al.* [2004] estimated the flux error reduction induced by upper tropospheric observations of CO_2 concentrations (their Figure 2c). Their results are based on simulated observations that are not restricted to the tropics. Their patterns over land are quite similar to our second configuration (Figure 8), despite a very different inversion set up. They differ significantly from our two estimates (Figures 4 and 8) over the oceans, since they show a minimum in the tropical Atlantic for the error reduction,

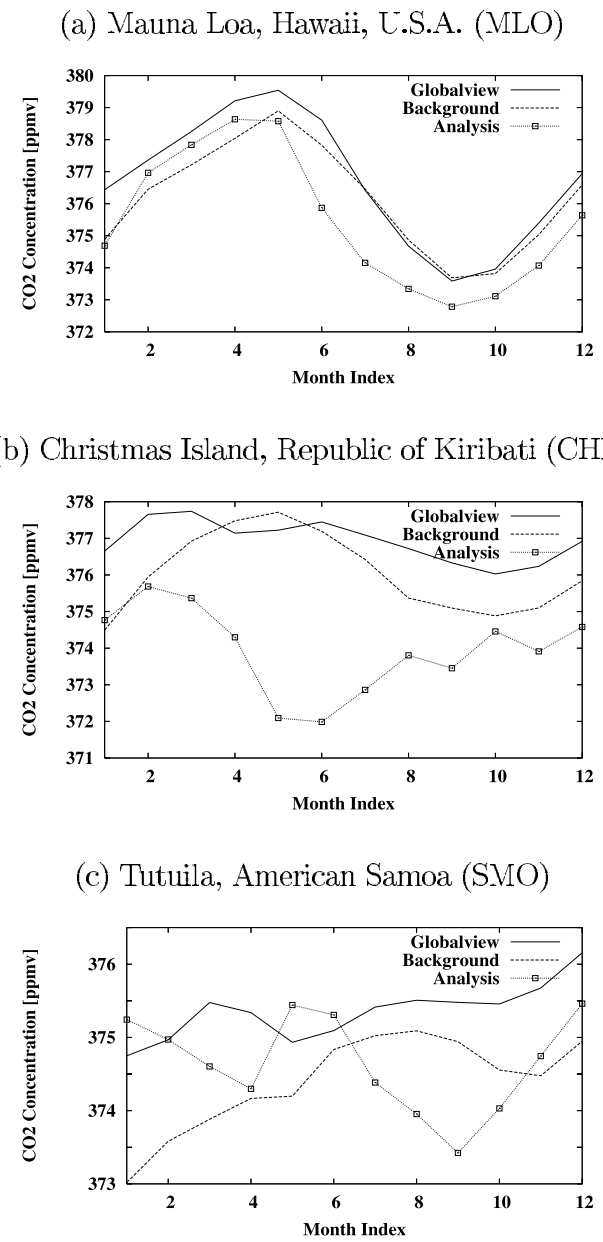

Figure 7. The 1990 time series of monthly mean CO_2 concentrations, in ppm, at three ground stations in Globalview, for the background and for the analysis. The Globalview identifier used in Table 1 is given in parenthesis.

where our two configurations consistently show a maximum. The very large correlation lengths used by Houweling and his coauthors (1250 and 2000 km over land and ocean, respectively) may explain the contradiction (S. Houweling, personal communication, 2005).

6. Discussion

[58] The above results are an early step in inferring CO_2 surface fluxes from actual satellite observations. A variational scheme has been built that successfully processes satellite retrievals over long periods of time (here 1 year) and without averaging the data over weeks or months as is usually done. The inversion system behaves consistently with the specifications of the inversion problem. However, the evaluation of the inferred fluxes indicates that these are less accurate than the prior fluxes given by a climatology. Our conclusion is that some of the inputs of the inversion scheme (observations, prior information, and/or corresponding errors) are not consistent with each other.

[59] The key inconsistent assumption that is violated is that there are no regional biases in the TOVS observations. Indeed, systematic errors have been previously found in the TOVS data set that cannot be resolved from the information contained in the TOVS radiances alone. It should be emphasized that the density of satellite measurements limits the impact of random errors and that consequently even poor-quality satellite retrievals should be superior to the existing flask network [*Rayner and O'Brien*, 2001]. However, biases are damaging and should be removed or at least minimized. In practice it is difficult to envisage a bias-correction scheme given the lack of high-quality column-integrated CO_2 observations. Further, one might not trust the prior information enough to bias-correct the observations against it as is done in the field of numerical weather prediction [*Harris and Kelly*, 2001]. A close collaboration between the people involved at some stage in the process of going from the raw satellite counts to elaborate products, like surface flux estimates, is required to diagnose and understand the sources of biases for a given satellite instrument.

Table 1. Year 1990 RMS Differences Between the Background (BG) or the Analysis (AN) and the Globalview (Obs) Monthly Means of Carbon Dioxide Concentrations, ppm, at Various Ground Stations[a]

Site	(Lat./Long.)	Obs. Std.	(BG-Obs) RMS	(AN-Obs) RMS
ALT	(82.5, −62.5)	5.2	3.5	3.7
MBC	(76.2, −119.3)	5.3	3.7	3.9
BRW	(71.3, −156.6)	6.1	3.7	3.8
STM	(66.0, 2.0)	5.0	1.4	1.4
CBA	(55.2, −162.7)	5.8	1.6	2.3
SHM	(52.7, 174.1)	6.0	1.2	1.8
CMO	(45.5, −124.0)	3.0	3.7	3.7
NWR	(40.0, −105.6)	2.6	6.2	6.5
AZR	(38.8, −27.4)	3.2	1.1	1.9
BME	(32.4, −64.7)	3.1	1.1	1.4
BMW	(32.3, −64.9)	2.8	1.0	1.5
MID	(28.2, −177.4)	2.7	1.0	1.5
KEY	(25.7, −80.2)	2.3	2.5	3.5
MLO	(19.5, −155.6)	1.9	0.8	1.4
KUM	(19.5, −154.8)	2.2	0.6	0.9
GMI	(13.4, 144.8)	2.4	1.3	2.5
RPB	(13.2, −59.4)	2.0	1.1	0.9
CHR	(1.7, −157.2)	0.5	1.2	3.2
SEY	(−4.7, 55.2)	0.9	1.5	1.3
ASC	(−7.9, −14.4)	1.0	1.3	1.7
SMO	(−14.2, −170.6)	0.4	1.1	1.1
CGO	(−40.7, 144.7)	0.7	1.6	1.0
PSA	(−64.9, −64.0)	1.1	1.7	1.0
SYO	(−69.0, 39.6)	0.7	1.9	1.5
HBA	(−75.6, −26.5)	0.7	1.6	1.2
SPO	(−90.0, −24.8)	0.7	1.3	1.0

[a]The observations are independent from the analysis. The offset averaged over all the stations has been removed before the RMS computation. Each station is defined by a three-letter acronym and a geographical position (latitude and longitude, in degrees). The standard deviation of the 12 Globalview monthly means is also indicated. Stations are ordered by decreasing latitude.

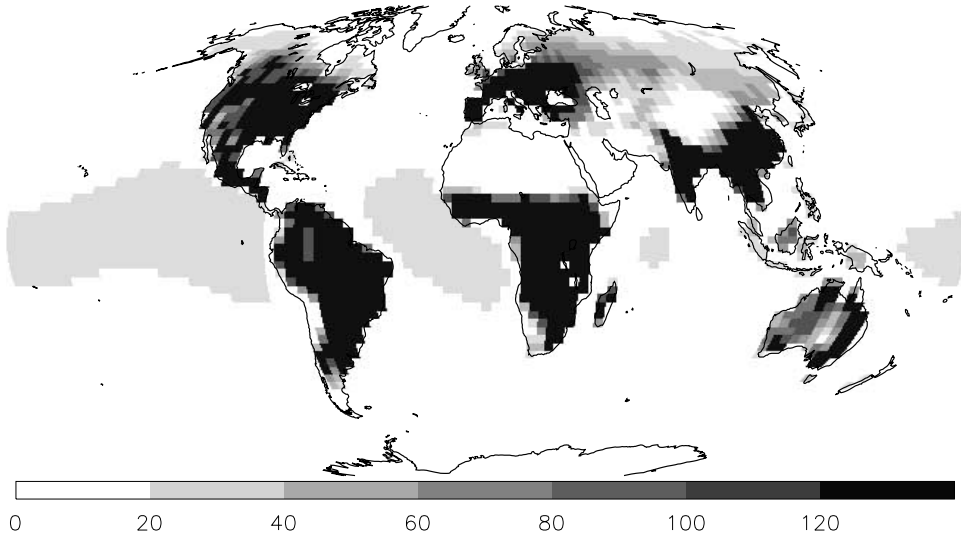

Figure 8. Truncated estimate of the reduction of CO_2 daytime flux errors (in g C per m^2 per year) for August 1990 and for the inversion using a physically based inversion matrix. The error reduction is defined as the square root of the difference between the background error variances and the analysis error variances. Note that a better convergence is obtained, which allows a better estimation of the eigenvectors. Therefore we use 14 eigenvectors here instead of 10 in Figure 4. This explains the larger figures.

[60] Our study also points at the sensitivity of the inferred fluxes to the prior information, despite the large amount of satellite retrievals (we processed individual measurements). Indeed, we find a large impact from changing the background errors. Their specification is important and should be refined in terms of variances, in terms of temporal correlations and in terms of spatial correlations.

[61] Last but not the least, errors of the atmospheric transport model may also degrade the inversion. In particular, the quality of the subgrid parameterizations (boundary layer turbulence and moist convection) may be essential, even though they suffer from large inaccuracies in current global models [e.g., *Chevallier and Kelly*, 2002].

7. Conclusion

[62] A Bayesian inference scheme has been set up to link satellite CO_2 retrievals to the CO_2 surface fluxes. A variational formulation has been chosen to cope with the large amount of satellite data. The scheme iteratively computes the optimum solution to the inference problem as well as an estimation of its error characteristics and some quantitative measures of the observation information content. The LMDZ model nudged with ECMWF winds provides information about the atmospheric transport to the inversion scheme. A surface flux climatology regularizes the inference problem.

[63] The first data set of satellite CO_2 retrievals from space, the one from TOVS established at LMD, has been used as a testbed for the whole method. The inferred fluxes are not judged realistic. We point at the sensitivity of the results to the formulation of the prior uncertainty and to the modeling of atmospheric transport. Most of all, regional biases in the observations hamper the inversion. On the one hand our study demonstrates the possibility to process the satellite CO_2 retrievals at high spatial and temporal resolutions. On the other hand it does not seem to be relevant for the TOVS data that would be more adequately used at very low resolution. The 26-year archive of TOVS data may be used in the future in surface flux inversion as a constraint on the monthly zonal means of CO_2 concentrations. In such an inversion configuration, surface measurements would also be assimilated to constrain the smaller horizontal scales. So far only the night-minus-day-difference (NDD) [*Chédin et al.*, 2005] of the TOVS retrievals has proved to carry a significant CO_2-related emission signal at the regional level, which could worth further exploitation to constrain the inversion of sources and sinks, provided that the transport model is adapted to simulate biomass burning-induced convection.

[64] The inversion scheme described here will allow us to investigate the use of the forthcoming CO_2 retrievals, like those of AIRS and OCO, that should be less prone to biases, at high resolution. Moreover, four-dimensional inversion schemes of this type could form the basis of ambitious multisensor data assimilation systems to estimate surface fluxes of key atmospheric compounds like CO_2, carbon monoxide, methane, or aerosols.

[65] **Acknowledgments.** Authors wish to thank R. Engelen (ECMWF), P. Rayner (LSCE), and F. Hourdin (LMD) for fruitful discussions, A. Idelkadi (LSCE) for help with the LMDZ model, and F. Marabelle (LSCE) for computer support. This study was cofunded by the European Union under project GEMS. Suggestions from two anonymous reviewers have helped to improve the clarity of the article.

References

Bai, Z., M. Fahey, and G. H. Golub (1996), Some large scale matrix computation problems, *J. Comput. Appl. Math.*, *74*, 21–89.

Bousquet, P., P. Peylin, P. Ciais, C. Quere, P. Friedlingstein, and P. Tans (2000), Regional changes in carbon dioxide fluxes of land and oceans since 1980, *Science*, *290*, 1342–1346.

Chédin, A., N. A. Scott, C. Wahiche, and P. Moulinier (1985), The Improved Initialization Inversion method: a high resolution physical method

for temperature retrievals from TIROS-N series, *J. Clim. Appl. Meteorol.*, *24*, 128–143.

Chédin, A., S. Serrar, A. Hollingsworth, R. Armante, and N. A. Scott (2003a), Detecting annual and seasonal variations of CO_2, CO and N_2O from a multi-year collocated satellite-radiosonde data-set using the new Rapid Radiance Reconstruction Network (3R-N) model, *J. Quant. Spectrosc. Radiat. Transfer*, *77*, 285–299.

Chédin, A., S. Serrar, N. A. Scott, C. Crévoisier, and R. Armante (2003b), First global measurement of midtropospheric CO_2 from NOAA polar satellites: Tropical zone, *J. Geophys. Res.*, *108*(D2), 4581, doi:10.1029/2003JD003439.

Chédin, A., R. Saunders, A. Hollingsworth, N. A. Scott, M. Matricardi, J. Etcheto, C. Clerbaux, R. Armante, and C. Crévoisier (2003c), The feasibility of monitoring CO_2 from high resolution infrared sounders, *J. Geophys. Res.*, *108*(D18), 4064, doi:10.1029/2001JD001443.

Chédin, A., S. Serrar, N. A. Scott, C. Pierangelo, and P. Ciais (2005), Impact of tropical biomass burning emissions on the diurnal cycle of upper tropospheric CO_2 retrieved from NOAA-10 satellite observations, *J. Geophys. Res.*, *110*, D11309, doi:10.1029/2004JD005540.

Chevallier, F., and G. Kelly (2002), Model clouds as seen from space: comparison with geostationary imagery in the 11 μm window channel, *Mon. Weather Rev.*, *130*, 712–722.

Chevallier, F., F. Chéruy, N. A. Scott, and A. Chédin (1998), A neural network approach for a fast and accurate computation of longwave radiative budget, *J. Appl. Meteorol.*, *37*, 1385–1397.

Crévoisier, C., S. Heilliette, A. Chédin, S. Serrar, R. Armante, and N. A. Scott (2004), Midtropospheric CO_2 concentration retrieval from AIRS observations in the tropics, *Geophys. Res. Lett.*, *31*, L17106, doi:10.1029/2004GL020141.

Dufour, E., and F.-M. Bréon (2003), Spaceborne estimate of atmospheric CO_2 column using the differential absorption method, *Appl. Opt.*, *42*, 3595–3609.

Engelen, R. J., and G. L. Stephens (2004), Information content of infrared satellite sounding measurements with respect to CO_2, *J. Appl. Meteorol.*, *43*, 373–378.

Engelen, R. J., E. Andersson, F. Chevallier, A. Hollingsworth, M. Matricardi, A. P. McNally, J.-N. Thépaut, and P. D. Watts (2004), Estimating atmospheric CO_2 from advanced infrared satellite radiances within an operational 4D-Var data assimilation system: Methodology and first results, *J. Geophys. Res.*, *109*, D19309, doi:10.1029/2004JD004777.

Errico, R. M. (1997), What is an adjoint model?, *Bull. Am. Meteorol. Soc*, *78*, 2577–2591.

Fisher, M. (2003), Estimation of entropy reduction and degrees of freedom for signal for large variational analysis systems, *Tech. Mem. 3497*, 18 pp., Eur. Cent. for Medium-Range Weather Forecasting, Reading, U.K.

Fisher, M., and E. Andersson (2001), Developments in 4D-Var and Kalman filtering, *Tech. Mem. 347*, 38 pp., Eur. Cent. for Medium-Range Weather Forecasting, Reading, U.K.

Fisher, M., and P. Courtier (1995), Estimating the covariance matrices of analysis and forecast error in variational data assimilation, *Tech. Mem. 220*, 26 pp., Eur. Cent. for Medium-Range Weather Forecasting, Reading, U.K.

Globalview-CO_2 (2004), Cooperative atmospheric data integration project—Carbon dioxyde (CD-ROM), NOAA, Boulder, Colo. (Also available on internet via anonymous FTP to ftp.cmdl.noaa.gov, path: ccg/co2/GLOBALVIEW).

Gurney, K. R., et al. (2002), Towards robust regional estimates of CO_2 sources and sinks using atmospheric transport models, *Nature*, *415*(6872), 626–630.

Harris, B. A., and G. Kelly (2001), A satellite radiance bias correction scheme for radiance assimiliation, *Q. J. R. Meteorol. Soc.*, *127*, 1453–1468.

Hourdin, F., and A. Armengaud (1999), Test of a hierarchy of finite-volume schemes for transport of trace species in an atmospheric general circulation model, *Mon. Weather Rev.*, *127*, 822–837.

Hourdin, F., and J.-P. Issartel (2000), Subsurface nuclear tests monitoring through the CTBT xenon network, *Geophys. Res. Lett.*, *27*, 2245–2248.

Hourdin, F., O. Talagrand, and A. Idelkadi (2005), Eulerian backtraking of atmospheric tracers: II Numerical aspects, *Q. J. R. Meteorol. Soc*, in press.

Houweling, S., F.-M. Bréon, I. Aben, C. Rödenbeck, M. Gloor, M. Heimann, and P. Ciais (2004), Inverse modeling of CO_2 sources and sinks using satellite data: A synthetic inter-comparison of measurement techniques and their performance as a function of space and time, *Atmos. Chem. Phys.*, *4*, 523–538.

Ide, K., P. Courtier, M. Ghil, and A. Lorenc (1997), Unified notation for data assimilation: Operational, sequential and variational, *J. Meteorol. Soc. Jpn.*, *75*, 181–189.

Kaminski, T., P. J. Rayner, M. Heimann, and I. G. Enting (2001), On aggregation errors in atmospheric transport inversions, *J. Geophys. Res.*, *106*, 4703–4716.

Lafont, S., L. Kergoat, G. Dedieu, A. Chevillard, E. Kjellström, U. Karstens, and O. Kolle (2002), Spatial and temporal variability of land CO_2 fluxes estimated with remote sensing and analysis data over western Eurasia, *Tellus, Ser. B*, *54*, 820–833.

Lanczos, C. (1950), An iteration method for the solution of the eigenvalue problem, *J. Res. Natl. Bur. Standards*, *45*, 255–282.

Laval, K., R. Sadourny, and Y. Serafini (1981), Land surface processes in a simplified general circulation model, *Geophys. Astrophys. Fluid Dyn.*, *17*, 129–150.

Law, R. M., P. J. Rayner, and Y. P. Wang (2004), Inversion of diurnally-varying synthetic CO_2: network optimization for an Australian test case, *Global Biogeochem. Cycles*, *18*, GB1044, doi:10.1029/2003GB002136.

Olivier, J. G. J., A. F. Bouwman, C. W. M. Van der Maas, J. J. M. Berdowski, C. Veldt, J. P. J. Bloos, A. J. H. Visschedijk, P. Y. J. Zandyelt, and J. L. Haverlag (1996), Description of EDGAR Version 2.0. A set of global emission inventories of greenhouse gases and ozone-depleting substances for all anthropogenic and most natural sources on a per country basis and on 1×1 grid, *RIVM Rep. 771060 002*, Natl. Inst. for Public Health and the Environ., Bilthoven, Netherlands.

Rayner, P. J., and D. M. O'Brien (2001), The utility of remotely sensed CO_2 concentration data in surface source inversions, *Geophys. Res. Lett.*, *28*, 175–178.

Rayner, P. J., R. M. Law, and D. M. O'Brien (2002), Global observations of the carbon budget, 3. Initial assessment of the impact of satellite orbit, scan geometry, and cloud on measuring CO2 from space, *J. Geophys. Res.*, *107*(D21), 4557, doi:10.1029/2001JD000618.

Rodgers, C. D. (2000), *Inverse Methods for Atmospheric Sounding: Theory and Practice*, 238 pp., World Sci., Tokyo.

Rödenbeck, C., S. Houweling, M. Gloor, and M. Heimann (2003), CO_2 flux history 1982–2001 inferred from atmospheric data using a global inversion of atmospheric transport, *Atmos. Chem. Phys.*, *3*, 1919–1964.

Rumelhart, D. E., G. E. Hinton, and R. J. Williams (1986), Learning internal representations by error propagation, in *Parallel Distributed Processing: Explorations in the Macrostructure of Cognition*, vol. 1, edited by D. E. Rumelhart and J. L. McClelland, pp. 318–362, MIT Press, Cambridge, Mass.

Sadourny, R., and K. Laval (1984), January and July performance of the LMD general circulation model, in *New Perspectives in Climate Modeling*, edited by A. L. Berger and C. Nicolis, pp. 173–197, Elsevier, New York.

Takahashi, T., et al. (2002), Global sea-air CO2 flux based on climatological surface ocean pCO2, and seasonal biological and temperature effect, *Deep Sea Res. II*, *49*, 1601–1622.

Tiedtke, M. (1989), A comprehensive mass flux scheme for cumulus parameterization in large-scale models, *Mon. Weather Rev.*, *117*, 1179–1800.

Tjemkes, S. A., and J. Schmetz (1997), Synthetic satellite radiances using the radiance sampling method, *J. Geophys. Res.*, *102*, 1807–1818.

Trémolet, Y. (2004), Diagnostics of linear and incremental approximations in 4D-Var, *Q. J. R. Meteorol. Soc.*, *130*, 2233–2251.

Turner, D. S. (1993), The effect of increasing CO_2 amounts on TOVS longwave sounding channels, *J. Appl. Meteorol.*, *32*, 1760–1766.

Turner, D. S. (1994), HIRS sensitivity to CO_2 mixing ratio and a pragmatic correction term, *J. Appl. Meteorol.*, *33*, 1155–1162.

Wanninkhof, R. (1992), Relationship between wind speed and gas exchange, *J. Geophys. Res.*, *97*, 7373–7382.

Weaver, A. T., J. Vialard, and D. L. T. Anderson (2003), Three- and four-dimensional variational assimilation with a general circulation model of the tropical Pacific Ocean, Part 1: formulation, internal diagnostics and consistency checks, *Mon. Weather Rev.*, *131*, 1360–1378.

P. Bousquet, F.-M. Bréon, F. Chevallier, P. Ciais, and S. Serrar, Laboratoire des Sciences du Climat et de l'Environnement, bat 701, L'Orme des Merisiers, F-91191 Gif-sur-Yvette Cedex, France. (frederic.chevallier@cea.fr)

A. Chédin, Laboratoire de Météorologie Dynamique, Institut Pierre-Simon Laplace, F-91128 Palaiseau, France.

M. Fisher, European Centre for Medium-Range Weather Forecasts, Shinfield Park, Reading RG2 9AX, UK.

P. Peylin, Laboratoire de Biogéochimie des Milieux Continentaux, BP 1, F-78850 Thivernal-Grignon, France.